Materials Science Forum
ISSN: 1662-9752, Vol. 1182, pp 13-22
doi:10.4028/p-PywJ3U

Submitted: 2025-12-19
Revised: 2026-02-09
Accepted: 2026-02-17
Online: 2026-04-10

The Influence of Side-Dependent and Nonlinear Bending Behavior in Forming Simulation of Non-Crimp Fabrics

Jan Paul Wank[1,a*], Levin Villing[1,b], Bastian Schäfer[1,2,c], Johannes Mitsch[1,d] and Luise Kärger[1,e]

[1]Karlsruhe Institute of Technology (KIT), Institute of Vehicle System Technology (FAST) – Lightweight Engineering, Rintheimer Querallee 2, 76131 Karlsruhe, Germany

[2]Simutence GmbH, Rintheimer Querallee 2, 76131 Karlsruhe, Germany

[a]jan.wank@kit.edu, [b]levin.villing@student.kit.edu, [c]bastian.schaefer@kit.edu, [d]Johannes.Mitsch@kit.edu, [e]luise.kaerger@kit.edu

Keywords: Non-Crimp Fabric, Forming Simulation, Bending

Abstract. Accurate prediction of forming behavior in dry textile reinforcements requires constitutive models that capture both in-plane and out-of-plane deformation mechanisms. This work presents the development and validation of advanced bending models for unidirectional non-crimp fabrics (UD-NCFs) that exhibit two distinct characteristics: side-dependent behavior arising from asymmetric stitching and glass fiber backing, and nonlinear behavior characterized by decreasing bending stiffness with increasing curvature. Based on cantilever bending tests with optical moment–curvature measurement, five mathematical formulations (piecewise linear, polynomial, power law, logarithmic, and exponential) used to describe the moment-curvature relation were systematically evaluated using the coefficient of determination R^2. The piecewise linear and logarithmic models achieved the highest accuracy, with R^2 values approaching unity across all fiber orientations and bending directions. These models were implemented in Abaqus/Explicit via the `VUGENS` user subroutine and validated through virtual cantilever tests, demonstrating good agreement with experimental deflection curves within the standard deviation bands. Application to hemispherical forming simulations revealed significant differences in wrinkle prediction between linear and nonlinear models. While the classical linear model based on Peirce predicted a single pronounced wrinkle in fiber direction, the nonlinear models captured additional wrinkles in the transverse direction and wider wrinkle patterns in fiber direction. Side-dependent models exhibited slightly increased wrinkle amplitudes compared to non-side-dependent models, particularly in fiber direction. The developed framework allows for a more accurate virtual process design than the current state of the art for composite forming operations by accounting for the side-dependent and nonlinear bending characteristics of UD-NCF materials.

1. Introduction

Finite element simulations have become a proven tool for analyzing process-induced deformations of textile reinforcements. They enable virtual process design and the prediction of forming defects such as wrinkles and fiber misalignment [1]. The predictive accuracy of these simulations strongly depends on constitutive models that describe both in-plane and out-of-plane deformation mechanisms. A detailed understanding of the forming behavior of engineering textiles is essential for minimizing forming defects during manufacturing and achieving optimal structural performance.

To simulate the forming behavior of textile reinforcements, experimental characterization must be performed. A standard test to characterize the bending behavior of textiles is the cantilever test according to [2]. This test provides a single bending stiffness value based on the overhang length of a fabric strip. When using optical measurement techniques, the bending moment-curvature relationship can be determined more accurately compared to the Peirce method [3]. The curve exhibits an initially linear region corresponding to elastic bending, followed by a degressive region at higher curvatures indicating nonlinear behavior. The Peirce bending stiffness, therefore, provides a reasonable approximation for small curvatures, while the nonlinear, degressive behavior at larger curvatures requires more advanced modeling approaches.

The ratio of bending stiffness to membrane stiffness is critical for the formation of wrinkles and other out-of-plane defects [4, 5]. This ratio governs the transition between in-plane deformation and out-of-plane buckling and is therefore a key parameter for forming simulation. The influence of bending stiffness on preforming has received increasing attention in recent years. [6, 7] and [8] showed that curvature-dependent, nonlinear bending laws are essential for predicting realistic wrinkle formation. [9] further observed a strong dependence of bending stiffness on curvature, temperature, and strain rate in unidirectional prepregs. These studies underline that nonlinear bending behavior must be included for a physically consistent representation of textile forming.

Despite these advances, most conventional bending models for dry reinforcements assume constant and side-symmetric stiffness. However, experimental findings on UD-NCFs reveal two key phenomena that are not captured in conventional models: a side-dependent bending response due to top-side asymmetric stitching and bottom-side glass fiber backing, and a pronounced nonlinear stiffness reduction at increasing curvature. These effects substantially influence wrinkle initiation and evolution during forming and must therefore be considered.

The present work addresses these limitations by developing and validating advanced bending models for UD-NCFs that explicitly account for side-dependent and nonlinear curvature-dependent behavior. Several mathematical formulations, including piecewise linear, polynomial, power-law, logarithmic, and exponential functions, are evaluated based on experimental cantilever bending tests. The most accurate models are implemented in Abaqus/Explicit using the `VUGENS` user subroutine and validated against experimental results. Hemispherical forming simulations are performed to analyze the influence of the new models on wrinkle formation and stiffness distribution.

2. Model Development for the Bending Behavior

Material characterization of the bending behavior. The investigated material is a unidirectional non-crimp fabric (UD-NCF) without binder, produced by Zoltek^{TM}. The reinforcement consists of PX35-50K continuous carbon fiber heavy tows, consolidated by a 76 dtex polyester (PES) yarn arranged in a tricot stitching pattern as shown in Figure 1 a). The fabric exhibits an areal weight of approximately $300\,\mathrm{g\,m^{-2}}$. Additionally, a thin layer of glass fiber yarns is integrated on the backside of the aligned fibers to enhance the fabric's stability and handling characteristics during forming operations (cf. Figure 1 b)).

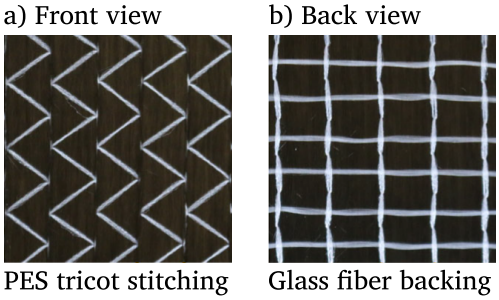

Fig. 1: Unidirectional non-crimp fabric from the a) front and b) back.

Cantilever bending tests were conducted by [10] to characterize the bending behavior of the UD-NCF material. The tests were performed on specimens with a width of $w_0 = 100\,\mathrm{mm}$, following the procedure outlined in the [11]. Each specimen was moved with a constant speed. The specimen bent under its own weight due to gravitational force. The specimen was moved until the first contact with the inclined surface with an incline angle of $\theta = 41.5°$ was established. The experiment was repeated six times for each configuration, using a new specimen for each repetition. The bending behavior was investigated in fiber direction ($0°$) and transverse to fiber direction ($90°$). Additionally, the tests were conducted with the front and back sides facing upwards. The back side is defined as the side with the

backing of glass fibers. The average experimental deflection curves for the different configurations are included in Figure 2.

To measure the nonlinear bending behavior, an optical measurement of the curvature and calculation of the bending moment was performed. This was done by [10] using an optical evaluation method proposed by [12]. The bending moment-curvature curves determined from the experimental deflection curves are included in Figure 3 for the configurations 0°-orientation front up and 0°-orientation back up. Detailed information regarding the experimental setup and evaluation procedure can be found in [10].

Modeling the side-dependent bending behavior. The 0°-orientation test resulted in a significantly higher bending stiffness compared to the 90°-orientation test. In the 90°-orientation test the load is mainly transmitted via the glass fiber backing and the stitching. It can be seen in Figure 2 that the overhang length is consistently higher when the front side is facing upwards.

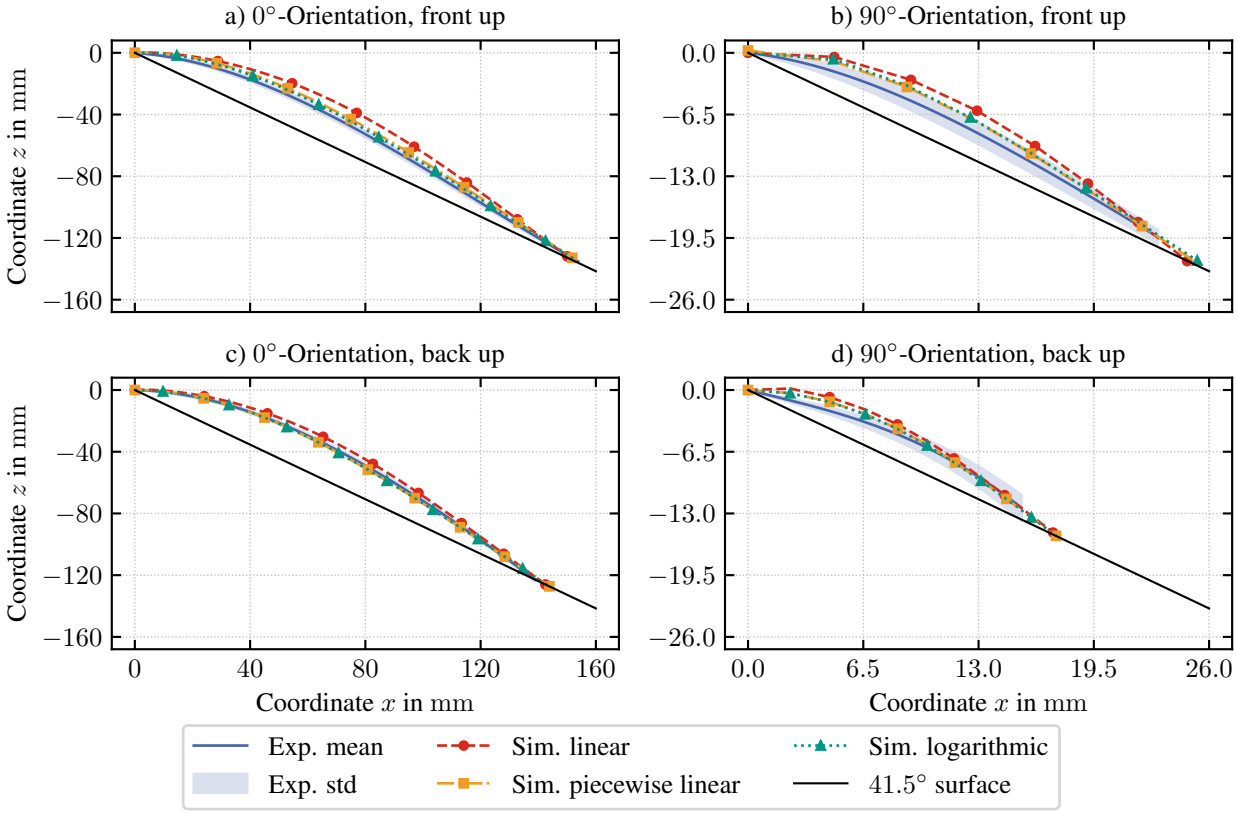

Fig. 2: Cantilever deflection curves: experimental (solid) and simulated (dashed) with different linear and nonlinear bending models for 0° (a, c) and 90° (b, d) orientations. The solid black line indicates the inclined surface of the cantilever test setup.

This can be attributed to the zigzag pattern of the stitching, as shown in Figure 1 a), which is under tension in these configurations and actively contributes to the bending stiffness. This is in contrast to the negligible stiffness of the stitching under compression. Therefore the experimental results indicate a side-dependent bending behavior of the material. This behavior is characterized by different bending moments and curvatures for the front and back sides of the material as shown in Figure 3 a) and b) for the 0°-orientation.

To capture the side-dependent bending behavior, a piecewise function is proposed. This model assumes different bending stiffness values for positive and negative curvatures, which correspond to the front and back sides of the material respectively. The mathematical description of the proposed model is summarized in Table 1.

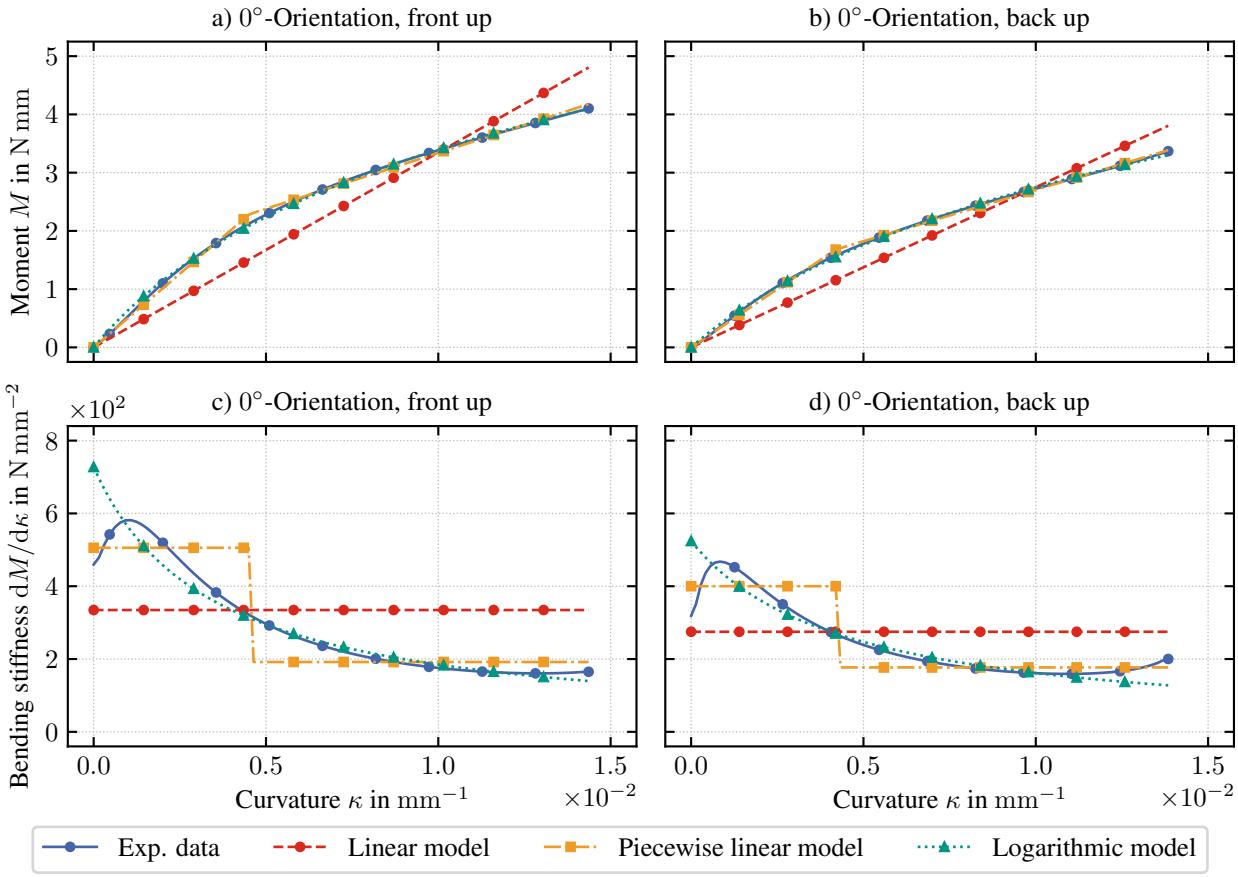

Fig. 3: Bending moment over curvature (a, b) and bending stiffness over curvature (c, d) for 0°-UD-NCF front up (a, c) and back up (b, d). Experimental data (solid) and model fits (dashed).

Modeling the nonlinear bending behavior. In addition to the side-dependent bending behavior, a nonlinear bending behavior is observed for both orientations of the UD-NCF material. This nonlinear behavior is evident from the experimental bending moment-curvature curves shown in Figure 3 a) and b). The bending stiffness-curvature curves in Figure 3 c) and d) further illustrate the nonlinear behavior, as the bending stiffness decreases with increasing curvature for the shown 0°-orientation. The experimental stiffness–curvature curves were obtained by numerical differentiation of the moment–curvature data. To capture this nonlinear bending behavior accurately, several mathematical functions are evaluated. These functions include a piecewise linear function, a second-order polynomial function, a power law function, a logarithmic function, and an exponential function. The mathematical descriptions are summarized in Table 2. The parameters of the different models are determined by fitting the bending moment-curvature curves obtained from the cantilever tests.

Table 1: Side-dependent bending models.

	Bending moment $M(\kappa)$
Fiber direction	$\begin{cases} B_1^{\mathrm{bu}}\,\kappa_1, & \kappa_1 < 0 \\ B_1^{\mathrm{fu}}\,\kappa_1, & \kappa_1 \geq 0 \end{cases}$
Transverse direction	$\begin{cases} B_2^{\mathrm{bu}}\,\kappa_2, & \kappa_2 < 0 \\ B_2^{\mathrm{fu}}\,\kappa_2, & \kappa_2 \geq 0 \end{cases}$

Table 2: Nonlinear bending models.

	Bending moment $M(\kappa)$
Piecewise linear	$\begin{cases} B\,\kappa, & \kappa \le \kappa_\mathrm{s} \\ B^s(\kappa - \kappa_\mathrm{s}) + B\,\kappa_\mathrm{s}, & \kappa > \kappa_\mathrm{s} \end{cases}$
2nd order polynomial	$a\,\kappa^2 + b\,\kappa$
Power law	$a\,\kappa^\mathrm{b}$
Logarithmic	$a\,\ln(1 + b\,\kappa)$
Exponential	$a\,b^\kappa$

Model validation and parameter identification of the developed bending model. A common measure of model accuracy is the coefficient of determination, R^2. It quantifies the proportion of variance in the observed data that is explained by the model and is defined as

$$R^2 = 1 - \frac{\mathrm{SSR}}{\mathrm{SST}} = \frac{\mathrm{SSE}}{\mathrm{SST}}, \tag{1}$$

where SST denotes the total sum of squares, SSE the explained sum of squares, and SSR the sum of squared residuals. These quantities are given by

$$\mathrm{SSE} = \sum_{i=1}^{n} (\hat{y}_i - \bar{y})^2, \quad \text{and} \quad \mathrm{SST} = \sum_{i=1}^{n} (y_i - \bar{y})^2. \tag{2}$$

Here, y_i represents the observed value at data point i, $\hat{y}_i$ the corresponding model prediction, $\bar{y}$ the mean of all observed values, and n the total number of data points. An R^2 value of 1 indicates a perfect model fit, meaning the model fully explains the observed variation.

In Figure 4 the R^2 values for the different developed bending models are presented for both fiber orientations and bending directions. The results indicate that the linear and the exponential functions are not suitable for capturing the nonlinear bending behavior of the UD-NCF material, as they yield low R^2 values across all configurations. Only for the $90°$-orientation with back side up a reasonable performance is observed because the bending moment-curvature curve in this configuration is almost linear. The other evaluated functions achieve consistently high R^2 values, indicating their capability to represent the nonlinear bending behavior accurately. Due to their consistently high performance for all configurations, the piecewise linear function and the logarithmic function are selected for description of the nonlinear bending behavior.

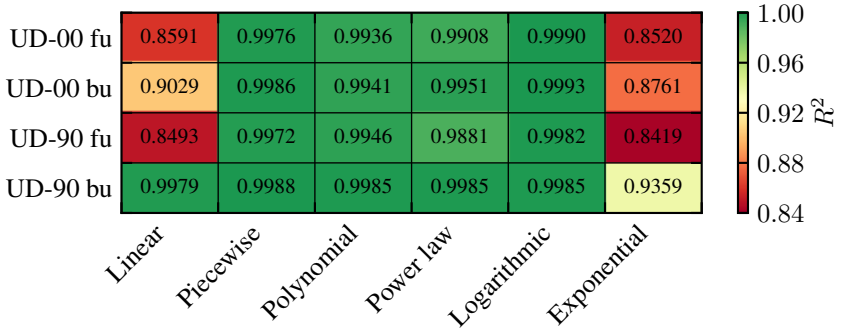

Fig. 4: Validation of the developed bending model in terms of the coefficient of determination R^2. A higher R^2 value indicates a better agreement with the experimental data.

The bending moment-curvature curves fitted with the piecewise linear function and the logarithmic function are shown in Figure 3 a) and b) for the $0°$-orientation with front side up and back side up, respectively, confirming the good agreement with the experimental data. Additionally, the linear bending moment-curvature curve obtained from the bending stiffness calculation according to [2] is included. The corresponding bending stiffness-curvature curves are shown in Figure 3 c) and d). For moderate curvatures, the derivation of the logarithmic model shows a better agreement with the experimental bending stiffness than the piecewise linear model. For low and high curvatures, the logarithmic model shows deviations from the experimental bending stiffness. The piecewise linear model exhibits constant bending stiffness up to the switching curvature κ_s, followed by a discontinuous stiffness drop at higher curvatures.

3. Validation on Coupon Test

Simulation setup. The cantilever bending tests are simulated using Abaqus/Explicit. The side-dependent and nonlinear bending models are implemented in the user-subroutine `VUGENS` previously developed by [12, 13]. The `VUGENS` subroutine enables direct specification of the moment-curvature relationship at each integration point. Given that the cantilever tests represent a pure bending load, membrane effects are not considered in the simulations. The Young's modulus $E^{\text{cant}}_{\text{analytical}}$ required for the `VUGENS` user subroutine is derived from the bending stiffness $B(\kappa)$ according to classical beam theory as

$$E^{\text{cant}}_{\text{analytical}} = \frac{B(\kappa)}{I} \tag{3}$$

with I being the area moment of inertia of the cantilever cross-section. The model geometry corresponds to the average experimental overhang length for each configuration. The specimen is discretized with `SR3` shell elements of approximate size $5\,\text{mm}$. Boundary conditions are defined with one edge fully fixed and the opposite edge free. Loading is applied as a gravitational force, represented by equivalent concentrated forces acting on all mesh nodes, reproducing the distributed specimen weight observed experimentally.

Comparison of experimental and simulation results. The deflection curves obtained from the cantilever tests for both $0°$- and $90°$-UD-NCF specimens are presented in Figure 2. The experimental results (solid lines) are compared to the simulation results (dashed lines) using the developed side-dependent, nonlinear bending models. The side-dependent, piecewise linear, and logarithmic bending models predict nearly identical deflection curves for all configurations. In contrast, the linear model following [2] consistently overestimates the deflection. Notably, at higher curvatures (corresponding to smaller values of the x-coordinate), the side-dependent, nonlinear models provide noticeably improved accuracy compared to the linear bending model. Overall, the simulated deflection curves lie within the experimental standard deviation bands, confirming the accuracy of the implemented bending formulations.

4. Demonstration on a Complex Forming Geometry

Simulation setup. The hemisphere forming tests are simulated using Abaqus/Explicit. The hemisphere forming test is a common benchmark for evaluating forming simulation approaches [13–15]. The simulation model is shown in Figure 5. The setup consists of a hemispherical punch with a radius of $75\,\text{mm}$ (green) and a flat die featuring a circular opening of radius $80\,\text{mm}$ (blue). No blankholders are used to intentionally promote the development of wrinkles during forming. Both the punch and die are modeled as discrete rigid surfaces. The punch motion is prescribed by a Dirichlet displacement boundary condition of $u_3 = 60\,\text{mm}$ in direction of $\boldsymbol{e}_3$, while the die is fully constrained in all translational and rotational degrees of freedom. The ply specimen is represented as a quadratic sheet with an edge length of $280\,\text{mm}$. The fibers are oriented in $\boldsymbol{e}_1$-direction. Therefore, due to symmetry of the problem, the setup can be simplified to model only one quarter of the entire configuration using symmetry boundary conditions along the planes defined by the $\boldsymbol{e}_1$- and $\boldsymbol{e}_2$-axes, as illustrated in Figure 5.

The edge length of the quarter-ply (beige) is 140 mm. The ply is discretized using a superimposed mesh of 3136 M3D3 and 3136 S3R elements with an element edge length of 5 mm. The superimposed element formulation with shared nodes is chosen to decouple the membrane and bending behavior of the fabric material [16]. The elements of the meshed ply are aligned along the fiber direction to prevent numerical intra-ply locking [17]. The ply represents a single layer of the UD-NCF material with a thickness of 0.4959 mm.

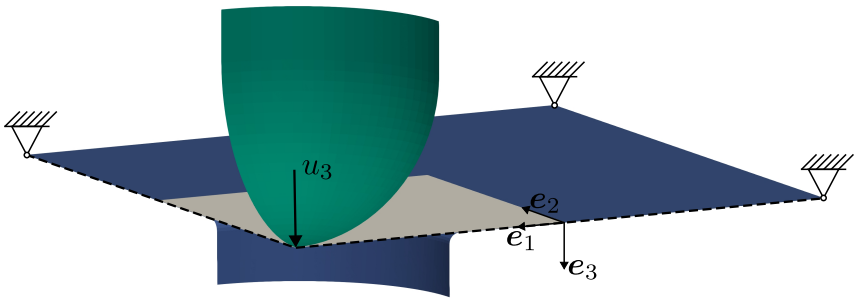

Fig. 5: Hemisphere forming simulation setup without blankholders, adopted from [10].

The membrane material response is modeled using a pseudo-invariant-based hyperelastic formulation according to [15], implemented via the user-defined material subroutine (VUMAT) and applied to the M3D3 elements. The bending behavior is described using the standard linear bending model of [2] as well as the developed side-dependent, nonlinear bending models, both implemented through the VUGENS subroutine and applied to the S3R elements. The tool–ply interaction is defined using the built-in general contact algorithm of Abaqus/Explicit.

Comparison of simulation results. The simulations were performed on an AMD EPYC 7313P system with 16 cores and 256 GB of RAM.

Each simulation was executed in parallel using 4 cores, resulting in an average computation time of approximately 2 min per simulation.

Figure 6 shows a comparison of the resulting displacement fields u_3, contrasting the models without side-dependency in a) with the models considering side-dependency in b). Due to symmetry, the result of the linear bending model in I is mirrored to fill the upper half. The nonlinear models II and III predict very similar wrinkle characteristics in terms of both location and amplitude. In the linear model I, a pronounced wrinkle appears in the $\boldsymbol{e}_1$-direction, caused by the fibers being aligned along $\boldsymbol{e}_1$, whereas in $\boldsymbol{e}_2$-direction only a slight indentation can be observed. In contrast, the wrinkles predicted by the nonlinear models in $\boldsymbol{e}_1$-direction are wider than those of the linear model, and the nonlinear models now predict a clearly developed wrinkle in $\boldsymbol{e}_2$-direction. The wrinkle amplitude is increased for the piecewise linear model II compared to the logarithmic model III, especially for the wrinkle in $\boldsymbol{e}_1$-direction. When comparing side-dependency effects, the non-side-dependent models in Figure 6 a) and the side-dependent models in Figure 6 b) show similar overall wrinkle patterns. However, the side-dependent models in Figure 6 b) exhibit a slightly increased wrinkle amplitude compared to the non-side-dependent models in Figure 6 a), with this effect being particularly noticeable for the wrinkle in $\boldsymbol{e}_1$-direction.

Figure 7 illustrates the stiffness distribution E_1 in the fiber direction $\boldsymbol{e}_1$ without differentiating whether the stiffness is used for positive or negative curvatures. For the linear model I in Figure 7 a), the stiffness remains constant because side-dependent and nonlinear effects are not captured. In contrast, the nonlinear models II and III in Figure 7 a) and b) show a stiffness variation depending on the curvature. Due to the continuity of the logarithmic function, the stiffness distribution of model III is smoother than that of model II, which is based on a piecewise definition. For small curvatures, the higher stiffness of model III compared to model II, as shown in Figure 3 c) and d), can be attributed to the shape of the underlying functions of the bending models. Overall, the results confirm that regions with low curvature exhibit lower stiffness values, whereas areas with higher curvature display

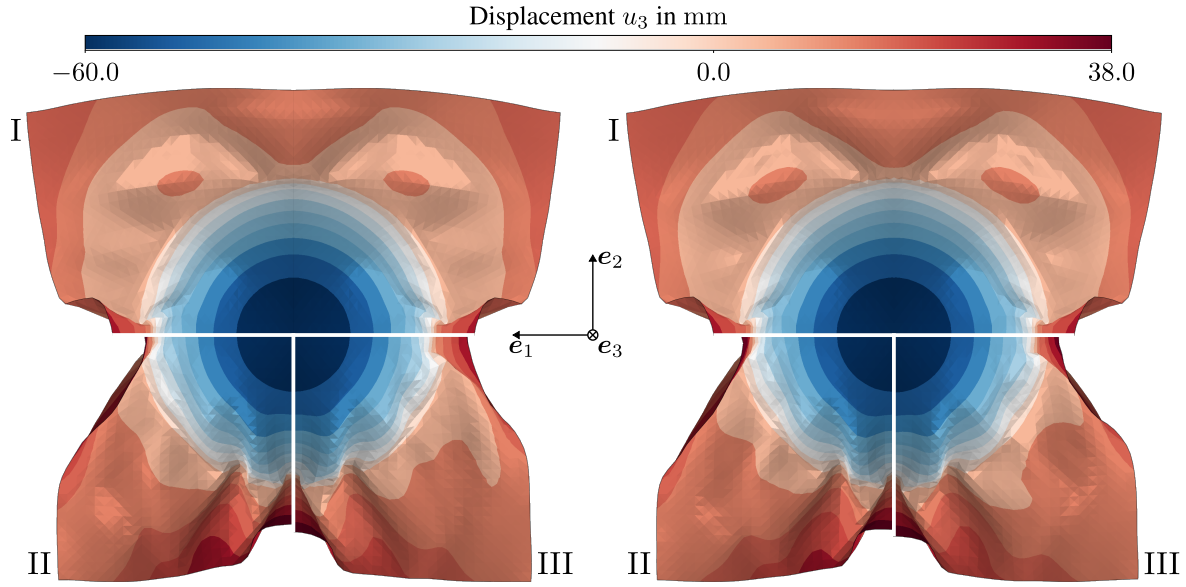

a) Without side-dependency b) With side-dependency

Fig. 6: Displacement field u_3 for the hemisphere forming test, comparing a) non-side-dependent and b) side-dependent bending models (I: linear Peirce, II: piecewise linear, III: logarithmic).

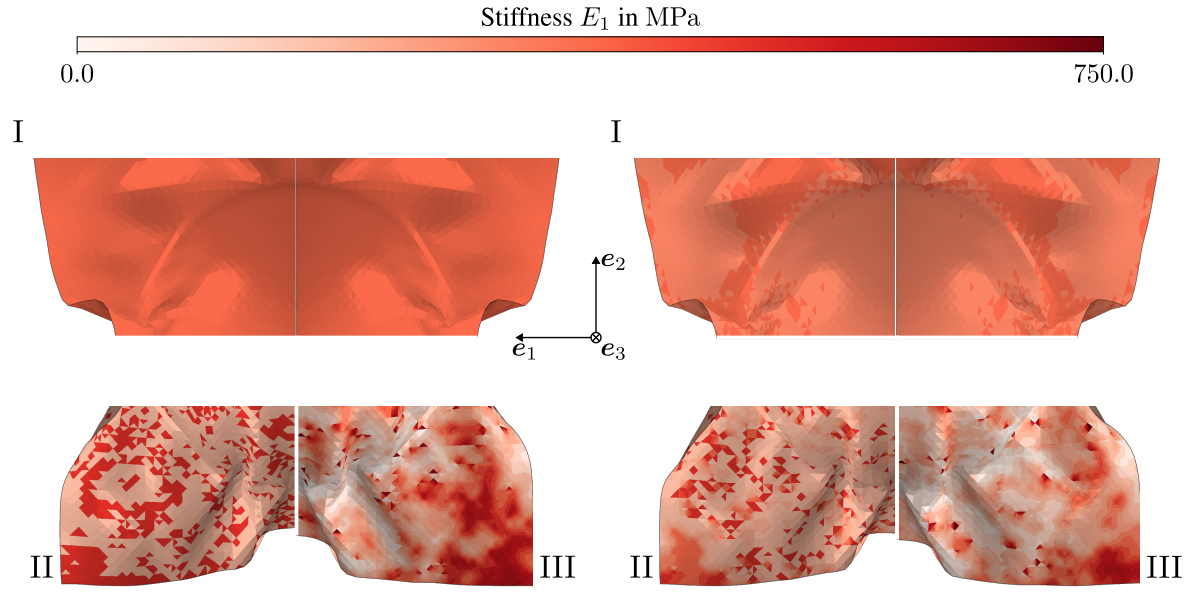

a) Without side-dependency b) With side-dependency

Fig. 7: Stiffness distribution E_1 (front-up/back-up) for the hemisphere forming test, comparing bending models a) without side-dependency and b) with side-dependency (I: linear Peirce, II: piecewise linear, III: logarithmic).

increased stiffness, as expected. When comparing side-dependency effects, the side-dependent models in Figure 7 b) show slightly lower stiffness values compared to the non-side-dependent models in Figure 7 a). The lower stiffness values for the side-dependent models correlate with the slightly increased wrinkle amplitudes observed for the side-dependent models in Figure 6. The logarithmic model is preferred over the piecewise linear model because it avoids stiffness jumps and is therefore more physically plausible.

5. Conclusion

This study presents the development and validation of advanced bending models to accurately represent the mechanical response of unidirectional non-crimp fabrics (UD-NCFs) during forming. Two key characteristics were identified and modeled: side-dependent behavior arising from the glass fiber backing that contributes to bending stiffness, and nonlinear bending behavior characterized by decreasing stiffness with increasing curvature. Several constitutive formulations were evaluated, among which the piecewise linear and logarithmic models achieved the highest accuracy, with R^2 values approaching unity across all fiber orientations and bending directions.

The models were implemented in Abaqus/Explicit via the `VUGENS` subroutine and validated against cantilever bending tests. The simulations showed good agreement with measured deflection curves. Both nonlinear formulations reproduced the experimental response within the experimental standard deviation, while the classical linear model by [2] consistently overestimated deflections, confirming the necessity of including nonlinear and side-dependent effects.

Application to hemispherical forming simulations demonstrated significant differences between the linear and nonlinear bending models in predicting wrinkle formation. While the linear Peirce model predicted a single pronounced wrinkle exclusively in fiber direction ($\boldsymbol{e}_1$), the nonlinear models captured additional wrinkles in the transverse direction ($\boldsymbol{e}_2$) and exhibited wider wrinkle patterns along $\boldsymbol{e}_1$. The piecewise linear and logarithmic models showed very similar wrinkle characteristics, with the piecewise model predicting slightly larger wrinkle amplitudes, especially along $\boldsymbol{e}_1$. The comparison of side-dependency effects revealed that side-dependent models exhibited slightly increased wrinkle amplitudes compared to non-side-dependent models, particularly in fiber direction. The predicted stiffness distribution reflected the expected curvature dependence, with the logarithmic model providing smoother transitions due to its continuous derivative.

Acknowledgements

The authors thank the Bundesministerium für Wirtschaft und Klimaschutz (BMWK, German Federal Ministry for Economic Affairs and Climate Action) for funding the "LuFo" research project "Efficient aerospace structures manufactured from carbon fiber-reinforced polymers using fully automated, linked and ultra-high-speed processes" (ELECTRA, project no. 20W1912D), for which the work was performed. This work is also part of the Heisenberg project "Digitalization of fiber-reinforced polymer processes for resource-efficient manufacturing of lightweight components" (project no. 455807141), funded by the Deutsche Forschungsgemeinschaft (DFG, German Research Foundation).

References

[1] L. Kärger, S. Galkin, C. Zimmerling, D. Dörr, J. Linden, A. Oeckerath, and K. Wolf, "Forming optimisation embedded in a CAE chain to assess and enhance the structural performance of composite components," *Composite Structures*, vol. 192, pp. 143–152, Jan. 2018.

[2] F. T. Peirce, "26—THE "HANDLE" OF CLOTH AS A MEASURABLE QUANTITY," *Journal of the Textile Institute Transactions*, vol. 21, pp. 377–416, Jan. 1930.

[3] E. Bilbao, D. Soulat, G. Hivet, and A. Gasser, "Experimental Study of Bending Behaviour of Reinforcements," *Experimental Mechanics*, vol. 50, pp. 333–351, Jan. 2010.

[4] P. Boisse, J. Colmars, N. Hamila, N. Naouar, and Q. Steer, "Bending and wrinkling of composite fiber preforms and prepregs. A review and new developments in the draping simulations," *Composites Part B: Engineering*, vol. 141, pp. 234–249, Jan. 2018.

[5] R. Bai, B. Chen, J. Colmars, and P. Boisse, "Physics-based evaluation of the drapability of textile composite reinforcements," *Composites Part B: Engineering*, vol. 242, p. 110089, Jan. 2022.

[6] F. Yu, S. Chen, J. V. Viisainen, M. Sutcliffe, L. T. Harper, and N. A. Warrior, "A macroscale finite element approach for simulating the bending behaviour of biaxial fabrics," *Composite Science and Technology*, vol. 191, Jan. 2020.

[7] F. Yu, S. Chen, L. Harper, and N. Warrior, "Simulating the effect of fabric bending stiffness on the wrinkling behaviour of biaxial fabrics during preforming," *Composites Part A: Applied Science and Manufacturing*, vol. 143, Jan. 2021.
[8] P. H. Broberg, E. Lindgaard, A. J. Thompson, J. P. H. Belnoue, S. R. Hallett, and B. L. V. Bak, "An accurate forming model for capturing the nonlinear material behaviour of multilayered binder-stabilised fabrics and predicting fibre wrinkling," *Composites Part B: Engineering*, vol. 274, p. 111268, Apr. 2024.
[9] Z. Zhao, K. Zhang, H. Cheng, Y. Zeng, and B. Liang, "Experimental characterization and numerical modelling of bending behavior of carbon fiber unidirectional thermoset prepregs," *Journal of Reinforced Plastics and Composites*, p. 073168442311613, Jan. 2023.
[10] B. Schäfer, *Macroscopic forming simulation of unidirectional non-crimp fabrics: Hyperelastic material modeling and 3D-solid-shell approach*. Doctoral Thesis, KIT, Karlsruhe, 2024.
[11] ASTM D1388-18 standard, "ASTM D1388-18: Standard Test Method for Determining the Flexural Stiffness of Medical Textiles," Apr. 2018.
[12] C. Poppe, T. Rosenkranz, D. Dörr, and L. Kärger, "Comparative experimental and numerical analysis of bending behaviour of dry and low viscous infiltrated woven fabrics," *Composites Part A: Applied Science and Manufacturing*, vol. 124, p. 105466, Jan. 2019.
[13] D. Dörr, F. J. Schirmaier, F. Henning, and L. Kärger, "A viscoelastic approach for modeling bending behavior in finite element forming simulation of continuously fiber reinforced composites," *Composites Part A: Applied Science and Manufacturing*, vol. 94, pp. 113–123, Jan. 2017.
[14] F. J. Schirmaier, D. Dörr, F. Henning, and L. Kärger, "A macroscopic approach to simulate the forming behaviour of stitched unidirectional non-crimp fabrics (UD-NCF)," *Composites Part A: Applied Science and Manufacturing*, vol. 102, pp. 322–335, Jan. 2017.
[15] B. Schäfer, D. Dörr, R. Zheng, N. Naouar, and L. Kärger, "A hyperelastic approach for modeling the membrane behavior in finite element forming simulation of unidirectional non-crimp fabrics (UD-NCF)," *Composites Part A: Applied Science and Manufacturing*, vol. 185, p. 108359, Oct. 2024.
[16] P. Boisse, N. Hamila, E. Vidal-Sallé, and F. Dumont, "Simulation of wrinkling during textile composite reinforcement forming. Influence of tensile, in-plane shear and bending stiffnesses," *Composites Science and Technology*, vol. 71, pp. 683–692, Jan. 2011.
[17] N. Hamila and P. Boisse, "Locking in simulation of composite reinforcement deformations. Analysis and treatment," *Composites Part A: Applied Science and Manufacturing*, vol. 53, pp. 109–117, Jan. 2013.

The publication of this article was funded by the Karlsruhe Institute of Technology 10.13039/100009133